Electrically silent potassium channel subunits from human lens epithelium

ALLAN R. SHEPARD AND JAMES L. RAE
Departments of Physiology/Biophysics and Ophthalmology, Mayo Foundation, Rochester, Minnesota 55905

Shepard, Allan R., and James L. Rae. Electrically silent potassium channel subunits from human lens epithelium. *Am. J. Physiol.* 277 (*Cell Physiol.* 46): C412–C424, 1999.—We describe the cloning and characterization of the first human members, hKv9.1 and hKv9.3, of the electrically silent delayed-rectifying-like K^+ channel subfamily. Their modulatory effects on the electrically active subfamily member hKv2.1 are also quantified. The hKv9 K^+ channels were isolated from a human lens epithelium cDNA library, but both hKv9.1 mRNA and hKv9.3 mRNA were found to coexist with the mRNA for hKv2.1 in a large number of human tissues. The hKv9.1 gene is composed of a minimum of five exons, with at least two alternatively spliced exons in the 5′-untranslated region (UTR). In contrast, the hKv9.3 gene is intronless across the coding region, 3′-UTR, and all of the analyzed 5′-UTR. Radiation hybrid mapping localized the hKv9.1 gene to 20q12 and the hKv9.3 gene to 2p24. Each electrically silent subunit, when coexpressed with hKv2.l, slows deactivation and inactivation compared with hKv2.1 expressed alone. In addition, each results in an increment in the single channel conductance.

delayed rectifier; hKv9.1; hKv9.3; transfection; Chinese hamster ovary cells

POTASSIUM CHANNELS ARE transmembrane proteins found in excitable and nonexcitable cells throughout the body and are essential for cell viability. Early studies resulted in a model of K^+ channels as simple homotetramers. During the past decade, many K^+ channels have been proven to be more diverse than the model. K^+ channel diversity arises from multiple genes, which may be alternatively spliced (10), from regulatory β-subunits (17), from the heteromultimerization of α-subunits (10), and from the recently identified K^+ channel-associated protein (32).

One family of K^+ channel α-subunits, comprising multiple genes, is activated on depolarization of the cell membrane and shows inactivation with variable time and voltage dependence depending on the gene involved. These channels are termed voltage-gated delayed rectifiers because of their short delay in activation after membrane depolarization. Recently, we cloned human Kv2.1 (hKv2.1), a member of this delayed-rectifying K^+ channel family, from human lens epithelium (HLEP) and transfected it into HEK-293 cells for expression (21). Although the hKv2.1 subunit made a current that clearly showed delayed rectification and voltage-dependent inactivation, the detailed properties of the current differed significantly from those of natural currents measured from human lens epithelial cells. Given the precedence for accessory subunits in the literature, we searched for other subunits with sequence homology to K^+ channels that might modify the properties of the hKv2.1 expressed in mammalian cells. We identified two previously unreported human cDNAs from a new subfamily of voltage-gated K^+ α-subunits, termed Kv9. The hKv9 amino acid sequences have all the expected features of the delayed-rectifier class of K^+ channel α-subunits including six hydrophobic transmembrane-spanning α-helical segments (S1-S6), an ion-selective pore region (H5), a leucine zipper motif between the S4 and S5 domains, and a positively charged amino acid every three amino acids in the S4 voltage sensor domain. Although we tentatively identified the cDNAs as coding for electrically active proteins, several observations proved inconsistent with this hypothesis. Overexpression of these cDNAs in transient transfections resulted in no current above background, despite the positive identification of transfected cells by cotransfection with a green fluorescent protein (GFP) plasmid. Fusion of these cDNAs with the cDNA for GFP resulted in poor targeting of the fusion protein to the plasma membrane but in accumulation in the perinuclear-reticular network and in a large ring structure near the plasma membrane. During the course of our investigations, we became aware of the literature describing new "electrically silent" α-subunits that modified the activity of other K^+ channel α-subunits with which they were coexpressed (2, 5, 9, 12, 18, 19, 25, 26, 31). As a result of these recently discovered subunits, delayed-rectifier α-subunits are now further subdivided into electrically active and electrically silent subunits (18, 26). Our "new" cDNAs proved to have homology to the cDNA of electrically silent channels cloned from other species, as indicated by a conservation of certain amino acid residues in the S6 transmembrane-spanning domain that differ from those in electrically active channels (26). Our subunits turned out to be the human homologues of Kv9.1 and Kv9.3, which had recently been cloned and expressed from mice and rats (18, 26).

We report here the cDNA cloning, tissue expression range of the mRNA, and chromosomal localization of the hKv9.1 and hKv9.3 genes, which are the first human members of the electrically silent, delayed-rectifying K^+ channel α-subunits cloned to date. We also describe the functional results after cotransfection of hKv2.1 with hKv9.1 or hKv9.3. We show that the properties of hKv2.1 are substantially altered by cotransfection with either of the electrically silent subunits and that the channels which result from cotrans-

The costs of publication of this article were defrayed in part by the payment of page charges. The article must therefore be hereby marked "*advertisement*" in accordance with 18 U.S.C. Section 1734 solely to indicate this fact.

fection are associated with currents whose properties much more closely match those of currents from HLEP than do those of the currents resulting from transfection with the cDNA for hKv2.1 alone.

METHODS

Cloning. Unless stated otherwise, standard molecular biology methodology was used (27). All plasmid constructions were checked by restriction mapping and sequencing. All enzymes and chemicals were purchased from GIBCO BRL (Gaithersburg, MD), Boehringer Mannheim (Indianapolis, IN), Sigma (St. Louis, MO), Stratagene (La Jolla, CA), Clontech (Palo Alto, CA), or New England Biolabs (Beverly, MA).

We constructed an oligo(dT)-primed cDNA library from the HLEP as previously described (21, 28). Degenerate oligonucleotide primers to the delayed-rectifier superfamily H5 and S6 domains corresponding to the conserved amino acids MTTVGY (5′-GGG**ATCGAT**ATGACNACNGTNGGNTA-3′; sense strand), TVGYGD (5′-GGG**ATCGAT**ACNGTNGGNTAYGGNGA-3′; sense strand), and PVPVIV (5′-GCG**CTCGAG**ACDATNACNGGNACNGG-3′; antisense strand) were synthesized with a terminal *Cla* I or *Xho* I restriction site (boldface) and used in single-side nested PCR amplification of HLEP plasmid cDNA libraries to generate sequence "tags" (21). PCR was performed on a 500-ng plasmid cDNA library (primary amplification) or a 1-μl primary PCR product (nested amplification) in 10 mM Tris·HCl, pH 8.3, 50 mM KCl, 1.5 mM $MgCl_2$, 0.25 mM deoxynucleoside triphosphates (dNTPs), 160 ng (primary amplification) or 600 ng (nested amplification) of each oligonucleotide, and 2.5 units of *Taq* polymerase (Boehringer Mannheim). The PCR sequence was 94°C for 1 min followed by 20 (primary amplification) or 40 (nested amplification) cycles of 94°C for 15 s, 56°C for 0 s, and 72°C for 0 s in a thermocycler (model 2400; Perkin-Elmer, Forest City, CA). A time of 0 s means that the thermocycler was allowed to ramp to the specified temperature but once there was immediately ramped to the next temperature. The nested amplified 129-bp PCR products were isolated, restriction digested, and subcloned into an appropriately digested pBluescript II (Stratagene) plasmid. Individual colonies were checked for correctly sized inserts and subsequently sequenced on both strands.

Individual-sequence tag sequences were subdivided into a centrally located 25-nt 5′-biotinylated capture oligonucleotide with 40-nt blocking oligonucleotides on either side. These oligonucleotides were combined and used to screen an HLEP cDNA library by our magnetic bead capture approach (29).

A full-length hKv9.1 open reading frame (ORF) clone with 5′- and 3′-untranslated regions (UTRs) was pieced together from three different captured cDNAs with various 5′ lengths. A 242-bp *Pst* I/*Bam*H I fragment containing a 5′-UTR and coding region, a 625-bp *Bam*H I/*Not* I fragment containing a coding region, and a 1,030-bp *Not* I/*Hin*d III fragment containing a coding region and a 3′-UTR were ligated into the *Pst* I/*Hin*d III sites of pCMV.SPORT1.βGal (GIBCO BRL), replacing the β-galactosidase gene to create pCMV.SPORT1.hKv9.1. A GFP fusion construct was prepared by first introducing a *Sal* I/Kozak sequence onto the 5′ end of the hKv9.1 ORF by PCR. PCR primers covering the hKv9.1 start codon and an internal *Bam*H I site 130 bp downstream were used to amplify a 137-bp product, which was subsequently purified and restriction digested with the *Sal* I/*Bam*H I fragment. The 3′ end of hKv9.1 was obtained from *Bam*H I-digested pCMV.SPORT1.hKv9.1. The 5′ *Sal* I/*Bam*H I and 3′ *Bam*H I/*Bam*H I ends of hKv9.1 were ligated into the *Sal* I/*Bam*H I sites of pEGFP-CI (Clontech).

An intact hKv9.3 ORF was obtained by RT-PCR of genomic DNA with primers spanning the start and stop codons: 5′-GGCATA**GTCGAC**GCCACCATGGTGTTTGGTGAGTTTTTCCAT-3′ and 5′-CTCATTATTT**GCGGCCGC**TCATTTTGCTGTGCAATTCTCCAAG-3′. The primers contained *Sal* I (5′ to start codon) and *Not* I (3′ to stop codon) restriction sites (indicated in boldface) and a Kozak consensus sequence surrounding the start codon to facilitate expression (11). The PCR product was restriction digested and cloned into the *Sal* I/*Not* I-digested pCMV.SPORT1 expression plasmid. A GFP fusion construct was prepared by subcloning the hKv9.3 *Sal* I/*Not* I insert from the pCMV.SPORT1 plasmid into the *Sal* I/*Not* I sites of the pEGFP-C1 vector (Clontech), which we engineered to include a *Not* I site in the multiple cloning site.

RT-PCR. First-strand cDNA synthesis was performed on 50 ng of mRNA (Clontech) with random primers according to the GIBCO BRL Superscript II protocol. Control reaction mixtures contained water in place of RT to control for genomic DNA amplification. PCR amplification was performed on 10% of the recovered first-strand cDNA or 1 ng of a human multiple-tissue cDNA panel (Clontech) with the following reaction components: 10 mM Tris·HCl, pH 8.3, 50 mM KCl, 1.5 mM $MgCl_2$, 0.2 mM dNTPs, 160 ng of each oligonucleotide, and 2.5 units of *Taq* polymerase (Stratagene) in a final 50-μl volume. Cycle conditions were 94°C for 1 min, followed by 22 [glyceraldehyde-3-phosphate dehydrogenase (GAPDH)] or 33 (hKv9.1, hKv9.3, and hKv2.1) cycles of 90°C for 10 s, 55°C for 0 s, and 72°C for 0 s; PCR was performed in a Perkin-Elmer model 2400 thermocycler. Primers were as follows: hKv9.1, TGTGGCCTGCAGTCATGTTT (sense) and CACTATGTACTAGGCCCTGT (antisense) (509 bp); hKv9.3, CCATGATGTGAGTACCGACTCCTC (sense) and GAACTCCGACATGCTGTGAACG (antisense) (220 bp); hKv2.1, GCCTTCACCTCCATCCTCAACT (sense) and ACTCATCGAGGCTCTGTAGCTCAG (antisense) (380 bp); GAPDH, CCATGGAGAAGGCTGGGG (sense) and CAAAGTTGTCATGGATGACC (antisense) (194 bp) (6). PCR products were run on a 3% agarose gel in the presence of 40 μg/l ethidium bromide and visualized with UV light. PCR products were isolated by QIAquick gel extraction (QIAGEN, Valencia, CA) and subjected to cycle sequencing to confirm their identities.

Construction of Kv2.1-Kv9 fusion proteins. Fusion genes encoding hKv2.1 and hKv9 were constructed in three steps. First, a linker encoding the flexible amino acid sequence (G4S)3 and containing 5′ *Bsr*G I and 3′ *Sal* I restriction sites was generated from the annealing of oligonucleotides 50182 (GTACAGGAGGCGGAGGCTCCGGCGGAGGAGGGTCCGGGGGCGGCGGAAGCG) and 50185 (CTCATTATTTTGTACAGATGCTCTGATCTCGTGTGCTT). The linker was cloned into the *Bsr*G I/*Sal* I sites of plasmid pEGFP-C1.1 (Clontech) to create plasmid pEGFP-C1.1-(G4S)3. Second, the hKv2.1 ORF was amplified by PCR with primers complementary to the start and stop codons and containing an *Nhe* I (start) or *Bsi*W I (stop) restriction site. The hKv2.1 PCR product was restriction digested and cloned into the *Nhe* I/*Bsr*G I sites of pEGFP-C1.1-(G4S)3 to create plasmid phKv2.1-(G4S)3. An error-free clone was identified by sequence analysis. Finally, the *Nhe* I/*Sal* I fragment of plasmid phKv2.1-(G4S)3 was subcloned into the *Nhe* I/*Sal* I sites of pEGFP-hKv9 plasmids, replacing the enhanced GFP genes. This created an in-frame hKv2.1-(G4S)3-hKv9 fusion gene with expression driven by the cytomegalovirus promoter.

Somatic cell hybrid PCR. Monochromosomal somatic cell (MSC) hybrid DNA (Quantum, Laval, PQ, Canada) was subjected to PCR amplification as recommended by the

manufacturer. Each PCR mixture consisted of 200 ng of individual somatic cell hybrid DNA, 1× PCR buffer (Boehringer Mannheim), 0.2 mM dNTPs, 2.5 units of *Taq* polymerase, and 160 ng of each primer in a total volume of 100 μl. Primers for hKv9.1 were identical to those used in RT-PCR analysis, and primers for hKv9.3 were GGGGTGTTTGTGCCTGTTTC (sense) and TGCATAAGCTGTAGCCACAAACC (antisense); both sets of primers correspond to the 3′-UTRs. Cycle conditions were 94°C for 3 min; 30 cycles of 94°C for 10 s, 60°C for 0 s, and 72°C for 0 s; and 72°C for 2 min. PCR was performed in a Perkin-Elmer model 2400 thermocycler. Amplification products were resolved on a 3% agarose gel in the presence of 40 μg/l ethidium bromide and visualized with UV light. PCR products were isolated by QIAquick gel extraction (QIAGEN) and subjected to cycle sequencing to confirm their identities.

Radiation hybrid (RH) mapping using the Stanford G3 human RH mapping panel (Research Genetics, Huntsville, AL) was performed with the same primers, cycle conditions, and amplification product analyses as for MSC hybrid PCR except that PCR mixtures consisted of 25 ng of each RH DNA and 16 ng of each primer in a total volume of 10 μl.

Amino acid alignment and phylogeny. Cloned K^+ channel amino acid sequences (see Fig. 5 and Table 1) were retrieved from the World Wide Web (WWW) by using the National Center for Biotechnology Information Entrez browser (www.ncbi.nlm.nih.gov/Entrez/). The conserved region between amino acids NVGG of the T1 domain and Y following the S6 domain (amino acids 55–464, hKv9.1; amino acids 20–413, hKv9.3) was selected from each subfamily member and aligned with the GeneWorks sequence analysis software, version 2.45 (IntelliGenetics, Mountain View, CA), a procedure which resulted in the phylogenetic tree shown in Fig. 5. Hydropathy analysis was performed by using the Kyte-Doolittle algorithm (13) with a window range of 11 amino acids.

Electrophysiology. Most patch-clamp measurements were made on Chinese hamster ovary (CHO) or HEK-293 cells after transfection with the cDNA for K^+ channel α-subunits. The cells were sealed with patch pipettes made from KG-12, 7052, or 8250 glasses pulled on a P-97 electrode puller (Sutter Instruments, Novato, CA). The electrodes were coated with R-6101 elastomer (Dow Corning, Midland, MI) and fire polished before use. Most of the patch-clamp measurements were standard (not perforated) whole cell measurements to minimize series resistance. For those cells whose capacitance (C_m) was routinely around 12 pF, we usually obtained series resistances (R_s) of 6–10 MΩ. These parameters result in an uncompensated bandwidth of $1/2\pi R_s C_m$ or ~2 kHz. This was adequate to resolve the time course for any of the currents we studied. However, the currents were often in excess of 10 nA, meaning that the voltage error with a 10-MΩ series resistance could be as large as 100 mV. Therefore, for all measurements we used 95–98% series resistance compensation to reduce the "effective" series resistance to <500 kΩ and thus the voltage error to <5 mV. In all cases, we used a compensation bandwidth that was at least five times our recording bandwidth. All measurements were made with an Axon Instruments (Foster City, CA) Axopatch 200B patch-clamp amplifier and a Digidata 1200B analog-to-digital interface by standard voltage protocols generated with PCLAMP software. The whole cell current was sampled at 2 kHz after being filtered through a 1-kHz eight-pole Bessel filter. The time course of current changes was fit usually with double exponentials by using CLAMPFIT (Axon Instruments). The 10–90% values reported represent the time required for the current to change from 10 to 90% of the difference between the current at the beginning and the end of the voltage pulse. Current-voltage (*I-V*) relationships were generated with custom software written in Excel (Microsoft, Redmond, WA).

Steady-state activation and inactivation were determined by using voltage steps to a series of voltages between 90 and −90 mV followed by a step to a −30-mV test voltage. In each case, the instantaneous current at −30 mV was plotted against the immediately preceding activating or inactivating voltage. The current was normalized between 0 and 1, and the normalized *I-V* relationship was fit with a Boltzmann distribution by using CLAMPFIT. For steady-state activation, the activating voltages were applied for 200 ms, whereas for steady-state inactivation they were applied for 60 s.

For noise reduction purposes, the single channel measurements were made with Corning 7760 glass (20). The pipettes were coated with R-6101 elastomer to within 100 μm from the tip. Short Axon Instruments electrode holders were used, again for noise reduction. Channel current was generally filtered at 2 kHz through an eight-pole Bessel filter and sampled at 4 kHz. The single channel *I-V* relationships were determined by using voltage ramps with 150 mM K^+ salts on both sides of the channels. The channel conductance was determined from the slope of the *I-V* relationship by using all of the points within ±20 mV of the reversal potential where the conductance was linear (see RESULTS for more details).

The solutions used and the compositions of their components (in mM) were *1*) normal Ringer: 149.2 NaCl, 4.74 KCl, 2.54 $CaCl_2$, 5.0 HEPES, 10 glucose; *2*) pipette-filling solution: 140 $KMeSO_4$, 10 KCl, 5 HEPES, 2 EGTA; and *3*) high-K^+ Ringer: 150 KCl, 2.54 $CaCl_2$, 5.0 HEPES, 10 glucose.

Transfection of CHO and HEK-293 cells. The hKv9.1 mammalian expression plasmid was transiently cotransfected with the pEGFP-C1 GFP expression plasmid by the PFX-7 lipid technique (Invitrogen, Carlsbad, CA) into HEK-293 human embryonic kidney cells or CHO cells. Green fluorescing cells identified by fluorescence microscopy were subjected to whole cell patch-clamp analysis as previously described (22).

Imaging. CHO cells were grown on coverslips. They were transfected with plasmids containing the cDNA for the GFP-α-subunit fusion protein of interest and were maintained under culture conditions for 20–24 additional hours. The cells were then fixed with 10% neutral formalin for 30 min to 1 h, and the coverslip with adherent cells was then attached to a microscope slide with a low-fluorescence mounting medium. The cells were imaged and photographed on a LaserScan confocal microscope (Carl Zeiss, Thornwood, NY).

RESULTS

Isolation of two electrically silent voltage-gated K^+ channel α-subunits. We used PCR amplification of HLEP plasmid cDNA libraries with degenerate oligonucleotides corresponding to conserved amino acids in the H5 and S6 domains of delayed-rectifying voltage-gated K^+ channels. PCR-amplified products were then subcloned, and individual clones were sequenced to generate a sequence tag. Several tags were identified, with most tags matching previously cloned delayed rectifiers. However, two of the tags (later determined to be those for hKv9.1 and hKv9.3) appeared to encode novel channels, and their full-length cDNAs were isolated.

Using the sequence tag information, we synthesized gene-specific probes and used these probes to screen the HLEP cDNA library for cDNA clones by a rapid

magnetic bead capture approach (29). Nondegenerate, gene-specific oligonucleotide probes based on the tag sequence were synthesized. The sequence under the original degenerate primers was excluded from primer design because of its unreliability.

hKv9.1. A partial hKv9.1 cDNA was obtained fortuitously as a *Not* I/*Not* I fragment from a *Not* I oligo(dT)-primed HLEP cDNA library and consisted of a 3,413-bp cDNA with an endogenous *Not* I site interrupting the ORF. A preliminary screen of tissue abundance revealed greater expression of hKv9.1 in brain than in HLEP (data not shown). Thus we generated a cDNA library from human brain primed with a gene-specific primer to codons for the amino acid sequence FSHFYR. An *Mlu* I restriction site was placed on the oligonucleotide terminus instead of a *Not* I site because of the endogenous *Not* I site in hKv9.1. We obtained cDNA clones that extended the 5′ end of our original cDNA by 915, 925, or 1,195 bp depending on the splice variant used. This was sufficient to identify a single in-frame start codon with an upstream stop codon in all three variants.

The 4,603-bp hKv9.1 cDNA contains a 440-bp 5′-UTR, a 1,578-bp ORF that encodes a 526-amino acid (58.3 kDa) protein (Fig. 1*A*), and a 2,581-bp 3′-UTR including a polyadenylation signal sequence. The sequence surrounding the hKv9.1 start codon (TCCACCATGG) is in good agreement with Kozak consensus

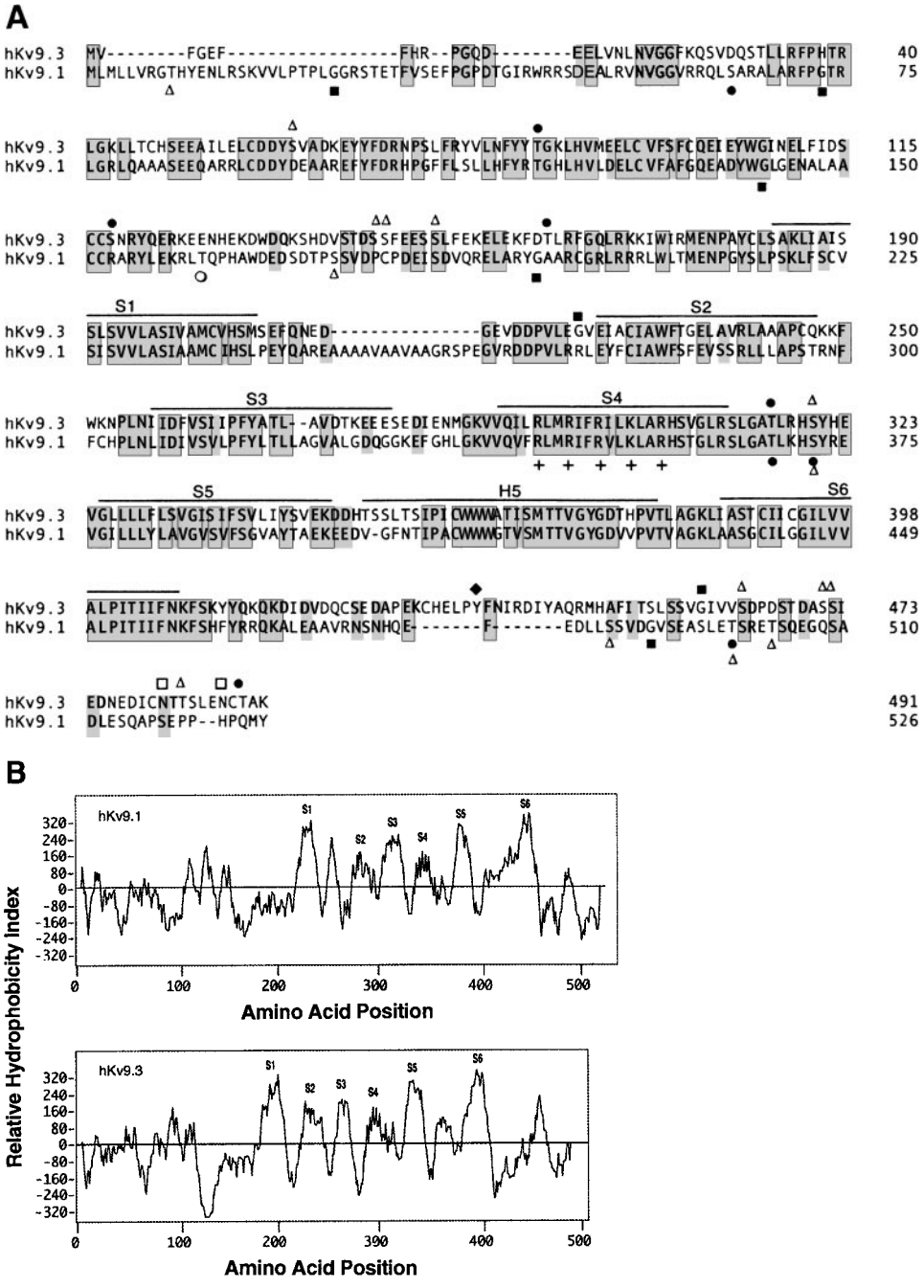

Fig. 1. Sequence comparison and hydropathy plots of hKv9.1 and hKv9.3. *A*: alignment of deduced amino acid sequences of longest open reading frames of hKv9.1 and hKv9.3 (GeneWorks). Identical amino acids (41%) are both shaded and boxed, and conserved amino acids are shaded. + Positively charged, voltage sensor amino acids in S4 segment. Putative hydrophobic transmembrane-spanning segments (S1–S6) and the pore region (H5) are overlined. Putative *N*-glycosylation (□), *N*-myristoylation (■), cAMP-dependent kinase (○), protein kinase C (●), casein kinase II (△), and tyrosine kinase (◆) sites are shown. *B*: Kyte-Doolittle hydropathy analysis (GeneWorks) of hKv9.1 and hKv9.3. Hydrophobic amino acids are positive, and hydrophilic amino acids are negative.

sequences (GCCRCCATGG) (11). The hKv9.1 cDNA ORF was found to be 82% identical to the newly cloned mouse Kv9.1 (mKv9.1) cDNA ORF (GenBank accession no. AF008573) at the nucleotide level and 84% identical at the amino acid level; thus hKv9.1 is the human homologue of mKv9.1. Interestingly, hKv9.1 contains an additional 31 amino acids on the amino terminus not found on mKv9.1. The significance, if any, of these additional amino acids is presently unknown. Our cDNA was submitted to GenBank (accession no. AF043473) and given the gene designation KCNS1 by the Human Genome Organization/genome database (HUGO/GDB) Nomenclature Committee.

To determine if the hKv9.1 gene contains introns and to verify that an intact mRNA exists in HLEP, we tried unsuccessfully to do genomic PCR and RT-PCR amplification with primers spanning the start and stop codons. Fortunately, a GenBank search revealed a 126,270-bp human 20q12–13.2 genomic P1 artificial chromosome (PAC) clone (clone 211D12; GenBank accession no. Z93016) that contained sequences perfectly matching our hKv9.1 cDNA sequence. We were able to deduce from the PAC clone sequence that the coding region and 3′-UTR of the hKv9.1 gene are composed of three exons, nt 26248–26326, 26792–27825, and 30147–33177 by the GenBank numbering, and that the 5′-UTR is composed of at least two exons, nt 24380–24566 and 25126–25317, which may be alternatively utilized. Identification of the hKv9.1 gene in this particular section of genomic DNA from 20q12–13.2 also independently confirmed our mapping results, described below, which we localized to the same region.

hKv9.3. An incomplete 1,378-bp hKv9.3 cDNA was obtained from a *Not* I oligo(dT)-primed HLEP cDNA library and included the 3′-UTR and a polyadenylation signal sequence. Inspection of the sequence indicated that we were likely missing ~200 amino acids or ~600 nt of 5′ sequence information based on homology to other delayed rectifiers. Thus a second HLEP cDNA library was generated, this time with a *Not* I primer containing degenerate, antisense nucleotides encoding the amino acid sequence PVPVIV. With this 5′-directed library, we isolated several clones and chose the one with the longest 5′ end to sequence. Sequencing this clone extended our 5′ sequence by 718 nt (196 amino acids), and the clone possessed an in-frame methionine within a strong Kozak sequence with several upstream stop codons.

The entire 2,097-bp hKv9.3 cDNA contained a 130-bp 5′-UTR, a 1,476-bp ORF that encodes a 491-amino acid (55.9 kDa) protein (Fig. 1*A*), and a 491-bp 3′-UTR that includes three ATTTA message destabilization sequences (1) and a polyadenylation sequence. A BLAST search revealed that the hKv9.3 ORF is 88% identical to the newly cloned rat Kv9.3 (rKv9.3) channel (GenBank accession no. AF029056) at the nucleotide level and 90% identical at the amino acid level (18); thus hKv9.3 is the human homologue of rKv9.3. Our cDNA sequence was submitted to GenBank (accession no. AF043472) and was given the gene designation KCNS3 by the HUGO/GDB Nomenclature Committee.

To determine if the hKv9.3 ORF contains introns, we performed genomic PCR. Multiple clones were sequenced, and the presence of an uninterrupted ORF and 5′- and 3′-UTRs was verified. All clones sequenced were identical except for a coding region single-nucleotide polymorphism at amino acid codon 450: either GCC encoding Ala or ACC encoding Thr (Fig. 1*A*).

Tissue distribution and gene structure of hKv9.1 and hKv9.3. To determine the gene expression patterns of hKv9.1 and hKv9.3, we performed PCR analysis on normalized human multiple-tissue cDNA panels purchased from Clontech (Fig. 2). PCR conditions were preoptimized, and PCR was performed under nonsaturating conditions (data not shown). hKv9.1 expression appeared greatest in adult and fetal brain, fetal kidney, fetal lung, prostate, and testis. hKv9.3 expression was greater in lung and more generalized than that of hKv9.1 but was noticeably absent from peripheral blood lymphocytes. hKv2.1 expression was greatest in adult and fetal brain, fetal skeletal muscle, and small intestine but was also absent from peripheral blood lymphocytes. Separate RT-PCR experiments using mRNA purchased from Clontech or prepared from HLEP cells showed hKv9.1 and hKv9.3 mRNA expression levels in HLEP to be roughly equivalent to adult kidney levels.

Chromosomal assignment of hKv9.1 and hKv9.3. hKv9.1 and hKv9.3 genes were localized to their unique chromosome in the human genome by MSC hybrid PCR analysis (Quantum) (Fig. 3*A*). With a single human chromosome in a rodent cell background, hKv9.1 was uniquely amplified from chromosome 20 and hKv9.3 was uniquely amplified from chromosome 2. Control amplifications from total human DNA but not hamster or mouse DNA indicated specificity for human and not rodent DNA. PCR product identity was confirmed by cycle sequencing.

RH PCR mapping (Research Genetics) was used to refine the localization of hKv9.1 and hKv9.3. Each PCR amplification product was scored as positive (1), negative (0), or ambiguous (R), and the results were submitted to the Stanford WWW RH mapping database for analysis (http://shgc-www.stanford.edu).

The raw RH scoring data for hKv9.1 make the likely cytogenetic location of the Kv9.1 gene the human chromosome band 20q12 (Fig. 3*B*) (7), whereas the raw RH scoring data for hKv9.3 suggest that the cytogenetic location of the Kv9.3 gene corresponds to human chromosome band 2p24 (Fig. 3*B*) (7).

Overexpression of hKv9.1 or hKv9.3 in transiently transfected heterologous cells. We performed transient transfections with the hKv9.1 or hKv9.3 cDNAs in appropriate mammalian expression vectors. We cotransfected with GFP-encoding plasmids to ensure identification of transfected cells for patch-clamp analysis. We saw no evidence of channel activity in any of the transfected cells examined. To identify technical incompatibilities, we tested $CaPO_4$-mediated coprecipitation vs. liposome-mediated transfection and we tested various cell types including tsA201, HEK-293, α-TN4, CHO, and COS-7 cells. We found no currents above

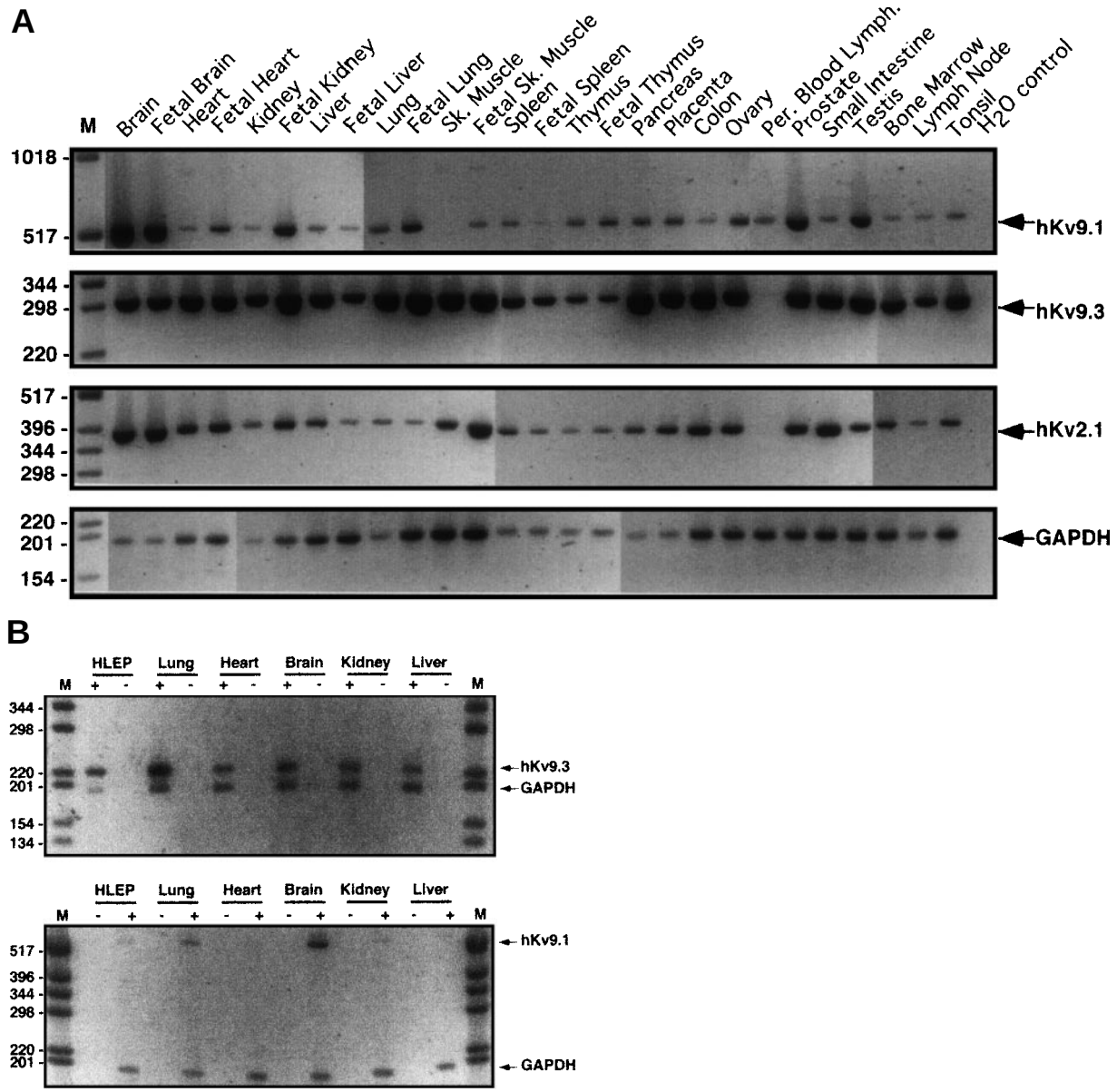

Fig. 2. mRNA expression pattern of hKv9.1 and hKv9.3 in human tissues. RT-PCR analysis was performed on human multiple-tissue cDNA (MTC) panels (Clontech) (*A*) or on cDNA generated from purchased mRNA (Clontech) or from freshly isolated mRNA from human lens epithelium (HLEP) (*B*). PCR amplification product sizes are 509 bp for hKv9.1 cDNA, 220 bp for hKv9.3 cDNA, 380 bp for hKv2.1 cDNA, and 194 bp for glyceraldehyde-3-phosphate dehydrogenase (GAPDH) cDNA. Individual channel and GAPDH PCR mixtures for each panel were loaded onto separate agarose gels (*A*) or combined in a single well for +/− RT reaction analysis on a single gel (*B*). Negative images are shown. Positions from the 1-kb DNA ladder (GIBCO BRL) markers are indicated. Sk., skeletal; per., peripheral; lymph., lymphocytes.

background after any of these approaches. Next, we fused the hKv9.1 or hKv9.3 ORF to the GFP ORF to create a GFP-channel fusion protein, which would allow us to image channel expression in transfected cells (Fig. 4). We concluded from the images that the majority of the hKv9.1 and hKv9.3 subunits were probably not reaching the plasma membrane but were instead trapped in some part of the synthetic process, as also observed for mKv9.1 (26). No obvious mitochondrial or endoplasmic retention signals were present in the hKv9.1 or hKv9.3 protein sequences to suggest specific targeting to these organelles. Thus it appears likely that an additional factor is involved in the trafficking and functioning of hKv9.1 and hKv9.3.

Overexpression of hKv2.1-Kv9 cotransfected pairs. As previously described for other electrically silent α-subunits (5, 9, 12, 18, 19, 26), we tested the modulatory effects of hKv9.1 and hKv9.3 on hKv2.1, which is the nearest evolutionary family member of the electrically active α-subunits (Fig. 5 and Table 1). To be sure that we had both hKv2.1 and Kv9 subunits coexpressed, we used a plasmid containing the cDNA for a fusion protein that included GFP and the Kv9 subunit of interest. This was cotransfected with a plasmid contain-

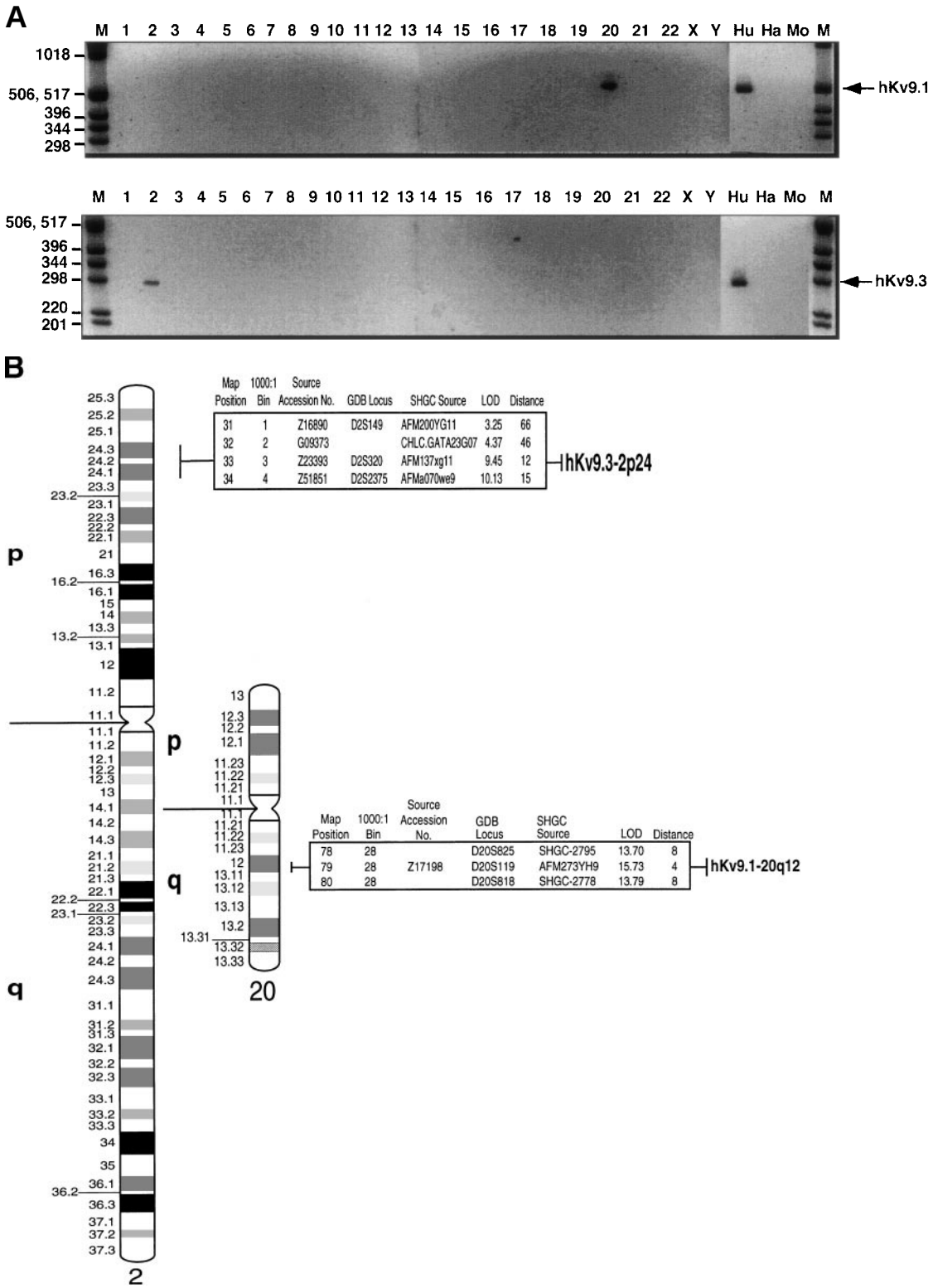

Fig. 3. Chromosomal localization of hKv9.1 and hKv9.3. *A*: monochromosomal somatic cell (MSC) hybrid PCR analysis (Quantum) of hKv9.1 and hKv9.3. Human chromosome numbers (1–22, X, Y) are indicated. Control reaction mixtures included whole-genome human (Hu), hamster (Ha), and mouse (Mo) DNA. Negative images are shown. Positions from 1-kb DNA ladder (GIBCO BRL) markers are indicated. *B*: ideograms of human chromosomes 20 and 2 (7) illustrating localization of hKv9.1 and hKv9.3 based on MSC and radiation hybrid (RH) mapping. Data at *right* were selected from Stanford Human Genome Center (SHGC) chromosome 2 or 20 RH map, version 2.0 (http://www.shgc-www.stanford.edu) and illustrate the linkage of hKv9.3 to AFM137xg11 and hKv9.1 to AFM273-YH9. Map position, overall best map position for the marker; 1,000:1 bin, ordering of markers within a bin at greater than 1,000:1 odds; source accession no., GenBank number for the STS source submission; GDB locus, GenBank locus for marker; SHGC source, SHGC source information; LOD, likelihood of odds for linkage; distance, distance in cR10000 between subject marker and linked marker.

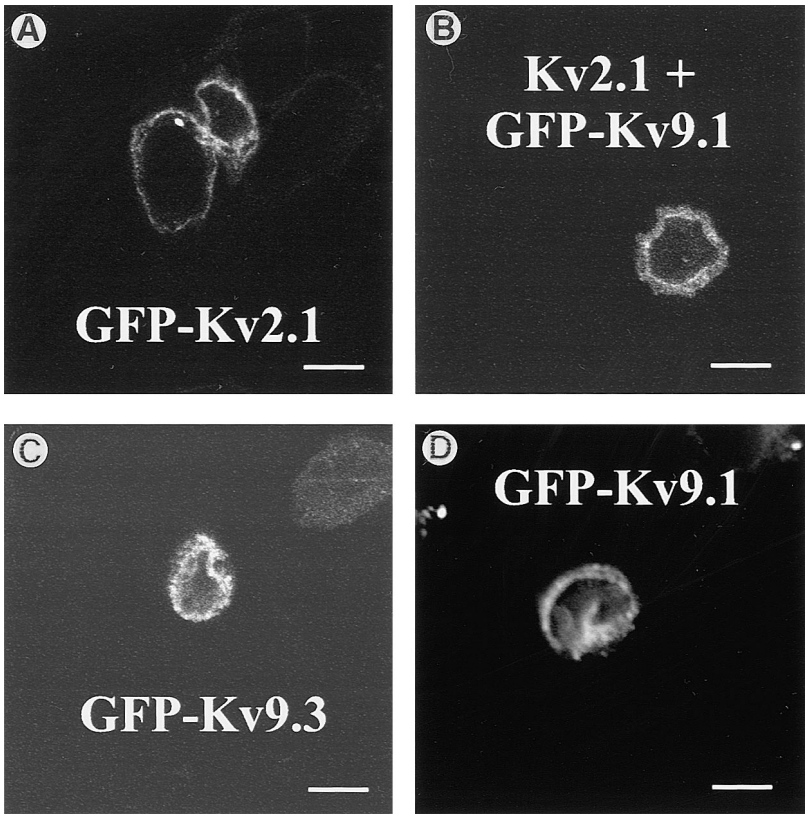

Fig. 4. Laser confocal microscope images of Chinese hamster ovary (CHO) cells expressing fusion proteins of green fluorescent protein (GFP) fused with hKv2.1 (*A*), hKv9.1 (*B*), and hKv9.3 (*C*). Localization to structures in addition to plasma membrane is obvious in all 3 panels but especially for *B* and *C*. Cells were photographed through a Zeiss ×100 oil planapochromatic objective. Calibration bars = 10 μM. *D*: cell photographed through a Nikon 1.2-numerical aperture point spread function water immersion objective and dehazed with Vaytek (Fairfield, IA) software.

ing the cDNA for hKv2.1. If a cell fluoresced, it had made the fusion protein and thus the Kv9, and if a current could be measured from the cell, it must also have expressed hKv2.1. Using cells so transfected, we quantified the time courses of activation, deactivation, and inactivation, steady-state activation, steady-state inactivation (using records such as those shown in Fig. 6), and single channel conductance. Where possible, we compared each quantified parameter to measurements obtained from natural currents in cultured human lens epithelial cells. Figure 7 plots 10–90% rise times of activation vs. voltage. In general, activation rise times from real lens currents and hKv2.1 alone match quite well, whereas the rise times from cotransfected hKv2.1 and hKv9.3 and cotransfected hKv2.1 and hKv9.1 clearly show a slowing of activation.

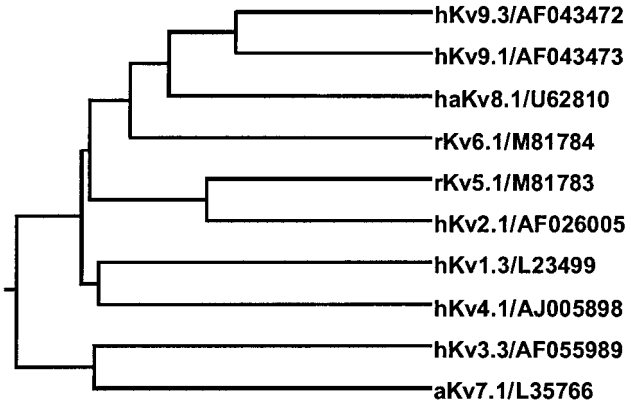

Fig. 5. Phylogenetic tree comparing hKv9.1 and hKv9.3 with selected members of each voltage-gated K^+ channel subfamily. Kv subfamily numbering is preceded by species (h, human; r, rat; ha, hamster; a, *Aplysia*) and followed by GenBank accession number. Silent subfamily members are Kv9.3, Kv9.1, Kv8.1, Kv6.1, and Kv5.1, and active subfamily members are Kv2.1, Kv1.3, Kv4.1, Kv3.3, and Kv7.1.

We further tested the activation time course by using CHO cells transfected with the cDNA for Kv2.1-Kv9.1 or Kv2.1-Kv9.3 fusion proteins. These constructs consisted of our usual expression plasmid into which was placed the cDNA for Kv2.1, a GGGGSGGGGSGGGGS spacer fused to its 3′ end, and either Kv9.1 or Kv9.3 cDNA fused to the 3′ end of the spacer. These constructs were meant to ensure 1:1 stoichiometry of Kv2.1 and one of the Kv9 subunits. The spacer was simply to separate the two fused subunits to keep them from interfering with each other. As can be seen in Fig. 7, when the stoichiometry of either Kv2.1-Kv9.1 or Kv2.1-Kv9.3 is constrained to 1:1, activation is slowed much less than when unfused Kv2.1-Kv9.X subunits are cotransfected.

Figure 8 plots 10–90% decay times of deactivation vs. voltage. Two important points are clear. First, hKv2.1 transfected alone clearly deactivates faster at almost all voltages than do the others shown. Second, the cotransfected hKv2.1 and hKv9.1 produce a pretty good match to the 10–90% decay times determined from real HLEP. Cotransfected hKv2.1 and hKv9.3 tend to be even slower, but the results are not statistically significant. It is interesting to note that the variances of the channel parameters obtained from cotransfection experiments are significantly greater than those from natural lens currents or from transfection with Kv2.1 alone. This is likely because, in the cotransfection experiments, the stoichiometry of subunit interaction can vary from one cell to another and because, even

Table 1. *Amino acid identities of hKv9.1 and hKv9.3 α-subunits with representative members of different voltage-gated K^+ channels*

hKv1.3	hKv2.1	hKv3.3	hKv4.1	rKv5.1	rKv6.1	Kv7.1	haKv8.1	hKv9.1	hKv9.3	
100	35	34	33	33	31	30	28	33	32	hKv1.3
	100	37	38	43	43	37	47	41	48	hKv2.1
		100	32	35	32	37	30	26	32	hKv3.3
			100	31	35	24	36	34	32	hKv4.1
				100	34	33	37	29	39	rKv5.1
					100	24	39	29	29	rKv6.1
						100	32	29	30	aKv7.1
							100	41	46	haKv8.1
								100	51	hKv9.1
									100	hKv9.3

Values are percent homologies calculated from conserved T1 to S6 domains as described in METHODS. GenBank accession numbers for each K^+ channel are indicated in Fig. 5.

within a single cell, the channels may have variable subunit stoichiometries.

Figure 9 compares 10–90% decay times of inactivation. Clearly, transfected hKv2.1 produces currents that inactivate much more rapidly than do the natural currents from HLEP. Either hKv9.1 or hKv9.3, when cotransfected with hKv2.1, yields currents whose inactivation is slowed compared with that for hKv2.1 alone. Kv9.1 slows it enough to match the parameters measured from the currents in cultured human lens epithelial cells, but Kv9.3 does not. We again tested our fusion constructs for their abilities to slow inactivation. In this case, both the Kv2.1-Kv9.1 and the Kv2.1-Kv9.3 fusions produced slowing that was very similar to that produced when unfused subunits were cotransfected (Fig. 9). Surprisingly, neither hKv9.1 nor hKv9.3 appreciably affected relationships of steady-state activation vs. voltage or steady-state inactivation vs. voltage compared with hKv2.1 alone (Fig. 10) when cotransfected as independent subunits. These steady-state values are also similar to those reported previously from cultured human lens epithelial cells (3).

For single channel recordings, voltage ramps were used to obtain high-resolution *I-V* relationships from which single channel conductance could be measured. Measurements reported are primarily from cell-attached patches for which the pipette contains 150 mM K^+ and the cells have been bathed in 150 mM K^+ for 15–30 min. Presumably these cells have no transmembrane voltage and an internal K^+ concentration approaching 150 mM. However, for each class of channels, at least three single channel conductance determinations were made from either inside-out or outside-out patches for which symmetrical conditions could be assured. The ramp protocol allowed the holding voltage, the voltage just before the ramp, and the ramp parameters to be controlled. This flexibility was required to get single channel records since, because of the expression levels, each patch usually contained 6–10 channels. This number had already been limited by using small-tipped, highly fire-polished electrodes with resistances of 25–50 MΩ. The use of depolarized holding voltages allowed some channels in the patch to be inactivated. By adjusting the voltage just before the ramp, the probability that a channel would open during the ramp could be modified. These parameters were adjusted for each patch until single channel records were obtained. Ramps of ~160 ms in length allowed a reasonable fraction of sweeps to have a channel open for the duration of the ramp. Figure 11 shows an example of the only kind of records we used for single channel determination. In 12 sweeps, at least 1 was required to have the channel closed during the entire sweep and 1 was required to have the channel open during the entire sweep. Then a single subtraction of the two resulted in the open-channel current vs. voltage. Low-noise recording techniques were used, so a very high signal-to-noise ratio, such as that shown in Fig. 11, was routinely obtained. For all of the single channels recorded, the background noise was between 99 and 153 fA RMS (root mean square) at 5 kHz (values on Axopatch 200B noise meter), with a median of 128 fA. In almost every case, the background noise was that predicted from the thermal noise of the seal resistance, making these measurements as good as could be done with the seals obtained. When simply averaged, the conductances from the various subunit combinations and patch configurations were as follows (means ± SD): for hKv2.1 alone, 13.8 ± 1.9 pS (n = 12); for hKv2.1-hKv9.1, 15.4 ± 2.8 pS (n = 12); for hKv2.1-hKv9.3, 18.2 ± 4.0 pS (n = 28). Simple averages should distort any differences, however, because one would expect that in the cotransfected cases some channels would be constructed from homomeric hKv2.1 subunits and some from hKv2.1 and Kv9 subunits coexpressed at various stoichiometries. Recalculating the conductances after excluding all values of 13.8 pS or less (hKv2.1 alone) yields 17.4 ± 1.5 pS for hKv2.1-hKv9.1 (n = 7) and 19.7 ± 2.5 pS for hKv2.1-hKv9.3 (n = 23). Verification that Kv9 subunits increase the channel conductance over that for Kv2.1 alone comes from single channel conductance measurements obtained from both the Kv2.1-Kv9.1 and Kv2.1-Kv9.3 fusion proteins. Their conductances are 19.3 ± 1.4 pS (Kv2.1-Kv9.1; n = 20) and 20.9 ± 3.5 pS (Kv2.1-Kv9.3; n = 47). Clearly, both conductances are higher than that for Kv2.1 alone even when 1:1 stoichiometry is constrained.

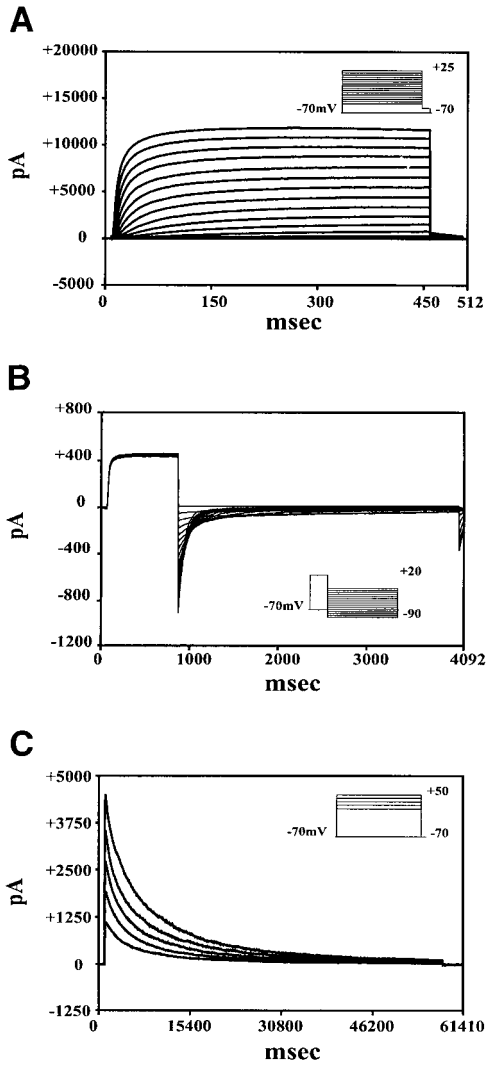

Fig. 6. Typical current records from transfected CHO cells used for quantifying activation (*A*), deactivation (*B*), and inactivation (*C*) time courses. Typical voltage protocols are shown in *insets*. Standard whole cell recording configuration included 95–98% series resistance compensation and a compensation bandwidth 5 times recording bandwidth. *A*: data resulting from Kv2.1 cotransfected with Kv9.3. *B*: data resulting from Kv2.1 cotransfected with Kv9.1. *C*: data resulting from cotransfection by Kv2.1 alone.

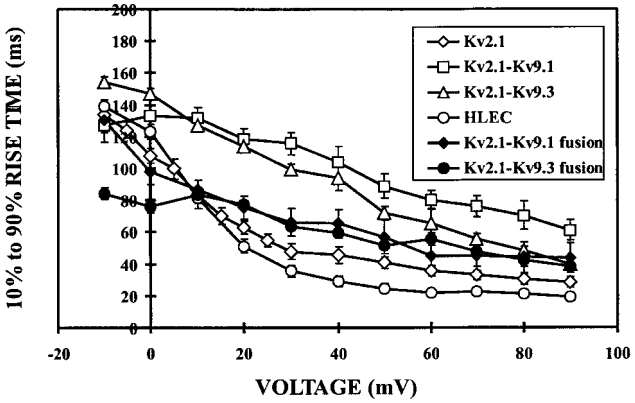

Fig. 7. Activation 10–90% rise times for currents from CHO cells transfected with hKv2.1 (n = 8–10 for voltages to −30 mV, n = 3 for 40–90 mV), hKv2.1 and hKv9.1 (n = 6), hKv2.1 and hKv9.3 (n = 12), Kv2.1-Kv9.1 fusion (n = 5), and Kv2.1-Kv9.3 fusion (n = 8) and for currents from cultured human lens epithelial cells (HLEC; n = 5). Records are from standard whole cell recording configuration. Values are means ± SD. Series resistance compensation = 95–98%.

DISCUSSION

The HLEP contains two previously unknown human delayed-rectifying K^+ channels, which we term hKv9.1 and hKv9.3. The genes for these two channel subunits reside at chromosomal locations 20q12 and 2p24, respectively. These channels, when expressed by themselves in transiently transfected mammalian cell lines, are apparently incapable of generating currents, at least with our procedures to date. However, coexpression of hKv9.1 or hKv9.3 with hKv2.1 does result in currents, but their kinetic properties are different from those of hKv2.1 when it is expressed without hKv9 subunits. One explanation might be that the hKv9 subunits are not targeted properly to the plasma membrane in the absence of hKv2.1 subunits. Evidence for this comes from imaging experiments with GFP-hKv9 fusion proteins expressed in mammalian cell lines. These fusion proteins appear to accumulate intracellularly and not preferentially in the plasma membrane when transfected alone, although such images do not have the resolution to show exclusion from the cell membrane. At best, they show much more accumulation in non-plasma membrane structures in the cell than that seen in cells expressing a GFP-hKv2.1 fusion protein. In our experiments, cotransfection of GFP-Kv9 proteins with Kv2.1 did not substantially reduce the apparent mistargeting to non-plasma membrane structures. Therefore, it is possible that the term electrically silent is a misnomer and what really happens is a failure of expression in the plasma membrane. Changes in the properties of Kv2.1 by coexpression with a Kv9 might be due to regulation by a different cell protein for which both Kv2.1 and a Kv9 are required or by an interaction between the subunits that does not require heteromultimer formation. Clearly, more work is needed on the targeting problem.

Our transfection results from CHO cells show both similarities and differences to those reported previ-

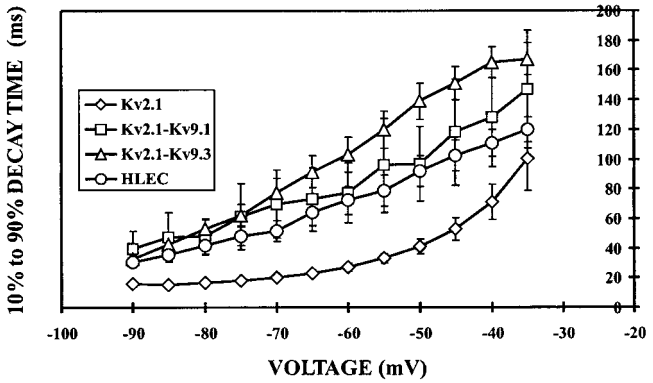

Fig. 8. Deactivation 10–90% decay times for currents from CHO cells transfected with hKv2.1 (n = 6), hKv2.1 and hKv9.1 (n = 3), and hKv2.1 and hKv9.3 (n = 14) and for currents from cultured HLEC (n = 6). Records are from standard whole cell recording configuration. Values are means ± SD. Series resistance compensation = 95–98%.

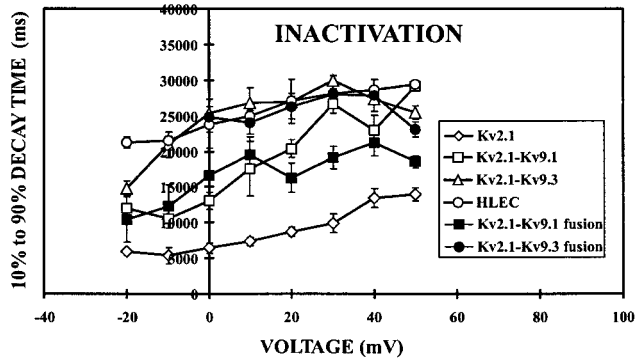

Fig. 9. Inactivation 10–90% decay times for currents from CHO cells transfected with hKv2.1 (n = 3), hKv2.1 and hKv9.1 (n = 5), hKv2.1 and hKv9.3 (n = 8), Kv2.1-Kv9.1 fusion (n = 4), and Kv2.1-Kv9.3 fusion (n = 6) and for currents from cultured HLEC (n = 11). Records are from standard whole cell recording configuration. Values are means ± SD. Series resistance compensation = 95–98%.

ously. We found that the current resulting from an hKv2.1-hKv9.1 or hKv2.1-hKv9.3 cotransfection had slowed activation compared with either current resulting from transfection with hKv2.1 alone or with the currents from cultured human lens epithelial cells. This discrepancy with data from human lens cells might suggest that hKv9.X subunits do not interact

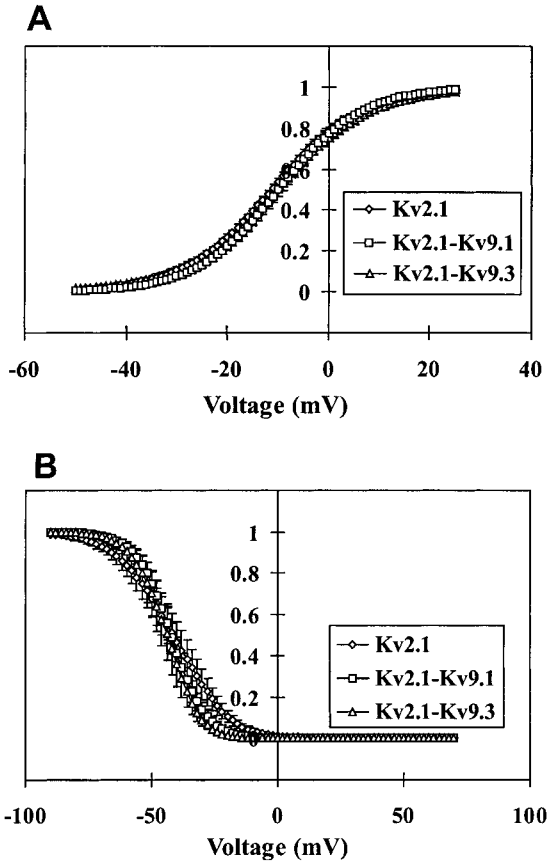

Fig. 10. Voltage dependence of steady-state activation (*A*) and steady-state inactivation (*B*) for CHO cells transfected with hKv2.12 alone, hKv2.1 and hKv9.1, or hKv2.1 and hKv9.3. Records are from standard whole cell recording configuration. Values are means ± SD. Series resistance compensation = 95–98%.

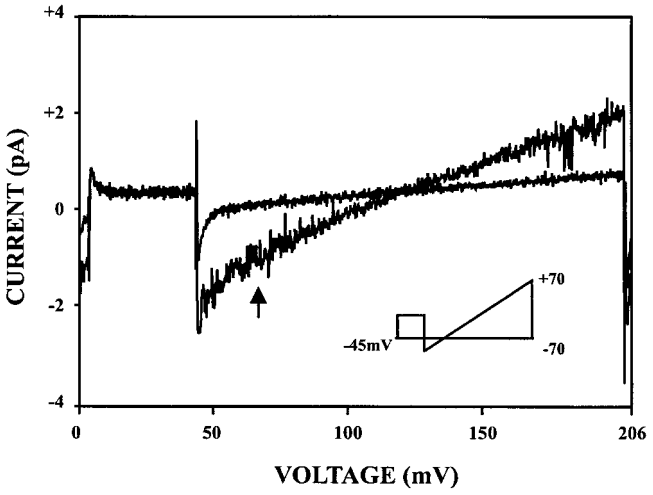

Fig. 11. Typical single channel current recordings during a ramp of voltage. Trace indicated by arrow is for channel open. Other trace is for channel closed. Voltage protocol is shown in *inset*. Holding potential and preramp potential were adjusted for each patch to maximize chance of getting single channel recording from multiple-channel patch.

with hKv2.1 subunits in human lens cells in vivo. However, expression of fusion proteins where hKv2.1 and hKv9.X are in 1:1 stoichiometry resulted in a much smaller reduction in activation time course than that with cotransfected nonfused subunits. Therefore, we cannot rule out the possibility that hKv9.1 slows activation only because we did not achieve the physiological stoichiometry with hKv2.1 in these experiments. Patel and coworkers (18), in fact, found that Kv9.3 subunits speed activation of Kv2.1 currents in *Xenopus* oocytes, and so there is as yet no consistent story concerning Kv9 subunits and activation.

In our experiments, both hKv9.1 and hKv9.3 slowed the deactivation and inactivation of hKv2.1-dependent currents, in keeping with previous results (18, 26). Interestingly, with the cotransfection of either electrically silent subunit with hKv2.1, inactivation and deactivation time courses more closely matched those measured from native human lens cells than did the time courses measured from hKv2.1 alone. Transfection with either hKv2.1-hKv9.1 or hKv2.1-hKv9.3 fusion proteins produces about the same slowing of activation as cotransfection of unfused subunits. These results, both activation and inactivation taken together, would support the notion that the in vivo channels in HLEP might be heteromultimers of hKv2.1 with one or more Kv9-type α-subunits. The most likely stoichiometry would seem to be 1:1. None of the different coexpression schemes for these subunits produced currents whose kinetics were a perfect match for those of the natural currents measured from real lens epithelial cells. There could be many reasons for this result. Perhaps we did not get the stoichiometry of the subunits correct. Perhaps lens epithelial cells and CHO cells produced different posttranslational modifications of the subunits. Perhaps there are other, as yet unknown, subunits involved or even other regulatory proteins. At present, we cannot be certain of the cause

of the small remaining mismatch. Unlike Patel and coworkers (18), we did not find that the voltage dependence of either open probability or inactivation was significantly shifted to the left in our expression system. However we, like previous workers (18), found that the electrically silent subunits increased the single channel conductance over that obtained with hKv2.1 alone. We cannot quantitatively compare our results to theirs because they chose to measure the conductance with asymmetrical (physiological) K^+ gradients, whereas we chose the symmetrical 150 mM K^+ condition. Still, the single channel results seem quite compatible when the differences are taken into account.

We believe that the best interpretation of all the data is that hKv2.1 subunits, when cotransfected with Kv9 electrically silent subunits, make heteromeric K^+ channels. We favor this model rather than a model in which hKv2.1 subunits make a homomeric channel which is modulated indirectly by the electrically silent subunits. Clearly, either view could explain the change in channel kinetics seen in coexpression studies. However, there is increasingly strong evidence that electrically silent subunits make heteromultimers with Kv2.1. The most highly studied electrically silent subunit to date, Kv8.1, has been shown to coimmunoprecipitate with Kv2.1 (9). Both Kv5.1 and Kv6.1 have been shown to associate with Kv2.1 in a yeast two-hybrid assay (12, 19). Although these results do not prove heteromultimerization, they are necessary criteria and highly suggestive. Kv2.1, when it is mutated to have its S6 sequence similar to that of Kv8.1, gives a channel which has kinetic properties similar to those of the channels formed when Kv2.1 and Kv8.1 are coexpressed. Moreover, the substantial alteration of the Kv2.1 single channel conductance that occurs with cotransfection would best be explained if the cotransfected electrically silent subunits were part of the channel pore because conductance is widely believed to be a pore-dominated phenomenon (4). Kv6.1, when coexpressed with Kv2.1, results in increasing the sensitivity of block by tetraethylammonium (TEA) (19). Because TEA is thought to bind in the pore of the channel (15), it is reasonable to believe that Kv6.1 might be part of the pore of a heteromultimer with Kv2.1. We made fusion proteins with one hKv2.1 subunit and one hKv9.1 or one hKv9.3 subunit. Castellano and coworkers (2) had previously made a tandem protein of Kv2.1 and Kv8.1. The cDNA for all three of these fusion proteins, when transfected into an expression system, made functional channels, suggesting that heteromeric channels are possible (comprising Kv2.1 and electrically silent subunits). None of these data absolutely prove that electrically silent subunits make heteromultimers with Kv2.1, but taken as a block, they strongly support that notion.

A variety of electrically silent K^+ channels have been cloned from a variety of species: rat Kv5.1, Kv6.1 (5), Kv8.1 (2), Kv9.1 (31), and Kv9.3 (18, 31); hamster Kv8.1 (9); and mouse Kv9.1 and Kv9.2 (26). A distinguishing feature of the electrically silent vs. electrically active Kv channels, as noted by Salinas et al. (26), is the presence of several absolutely conserved amino acid differences in the S6 transmembrane domain. Another interesting feature of electrically silent α-subunits is their relatively short COOH-terminal cytoplasmic tail (26). hKv9.1 and hKv9.3 also contain these sequence identifiers.

Rat Kv9.3 cloned from pulmonary arteries was identified as forming an oxygen-sensitive, ATP-dependent delayed-rectifying K^+ channel when associated with hKv2.1 (18). These authors showed that the presumed Kv2.1-Kv9.3 heteromultimer is open near the resting membrane potential of pulmonary artery myocytes and that its activity is controlled by internal ATP and inhibited by hypoxia, thus possibly playing a role in vasoconstriction and hypertension. The potential physiological role of human Kv9.3-Kv2.1 in the lens epithelium and other cell types remains to be elucidated; to date interactions with internal ATP and the effect of hypoxia have not been studied. The relatively high level of hKv9.3 in human lung suggests that it may play a role, similar to rat Kv9.3, in human pulmonary myocytes.

Mouse Kv9.1 and Kv9.2 mRNAs are present at high levels in the brain, as is rat Kv9.1 (31), and colocalize with Kv2.1 and Kv2.2 in several regions (26). Here we show that the mRNAs for hKv2.1 and hKv9 subunits coexist in many human tissues. In fact, it seems to be the rule, rather than the exception, that if hKv2.1 mRNA is found in a human tissue, so also is hKv9.1 and hKv9.3. In our lens cells, they all are found within a single cell type. Given that commercial cDNA from tissues does not come from a single cell type, one cannot be sure that all three subunits could be found in any one cell. However, it would now seem important to look for these or other subunits whenever Kv2.1 is found in any cell.

The changes in the kinetics of the Kv2.1 currents after coexpression with Kv9 subunits are quite subtle. It seems quite unlikely that those differences have much relevance in a lens epithelial cell that changes its transmembrane voltage slowly if at all. That is particularly true given that lens epithelial cells are connected to each other and to the lens fiber mass through gap junctions. This arrangement would ensure that any possible voltage changes would be blunted and slowed. The kinetic differences in the Kv2.1 currents with coexpression are most likely to have relevance in excitable cells where rapid changes in transmembrane voltage are inherent to their function. Nature seems to have conserved the multiple-subunit structure of these particular K^+ channels whether they are in epithelial cells or excitable cells. It does not follow, however, that the role of their kinetics in the physiology of the different cell types is conserved.

The localization of hKv9.1 to chromosome 20q12 warrants an investigation of the role of this gene in the phenotypic abnormalities of Fanconi's anemia (16) and maturity onset diabetes of the young (23) and in the increased chromosomal segment copy number in breast carcinomas (8).

hKv9.3 was localized to chromosome 2p24, which is a region associated with abnormal phenotypes such as

neural tube defects on triplication (14) and short stature, minor facial anomalies, microcephaly or anencephaly, hypotonia, mental retardation, and sensorineural hearing loss on deletion (24, 33). Hearing loss is an interesting phenotype to be associated with this region because homozygous mutation of another delayed-rectifier K^+ channel, KVLQT1, was shown to cause deafness in Jervell and Lange-Nielsen syndrome (30). hKv9.3 might be investigated as a candidate gene for these diverse phenotypic abnormalities.

We are grateful to Jerry Dewey, Sara Braun, and Helen Hendrickson for technical assistance, to Joan Bratcher for computing and analysis, and to Kristy Zodrow for manuscript preparation.

This work was supported by National Eye Institute Grants EY-03282 and EY-06005 and by the Mayo Foundation.

The use of specific products here does not constitute an endorsement of those products.

Address for reprint requests and other correspondence: J. L. Rae, Depts. of Physiology/Biophysics and Ophthalmology, Mayo Foundation, 200 1st St. S.W., Rochester, MN 55905 (E-mail: rae.james@mayo.edu).

Received 20 November 1998; accepted in final form 14 May 1999.

REFERENCES

1. **Akashi, M., G. Shaw, M. Hachiya, E. Elstner, G. Suzuki, and P. Koeffler.** Number and location of AUUUA motifs: role in regulating transiently expressed RNAs. *Blood* 83: 3182–3187, 1994.
2. **Castellano, A., M. D. Chiara, B. Mellstrom, A. Molina, F. Monje, J. R. Naranjo, and J. Lopez-Barneo.** Identification and functional characterization of a K^+ channel alpha-subunit with regulatory properties specific to brain. *J. Neurosci*. 17: 4652–4661, 1997.
3. **Cooper, K., P. Gates, J. L. Rae, and J. Dewey.** Electrophysiology of cultured human lens epithelial cells. *J. Membr. Biol*. 117: 285–298, 1990.
4. **Doyle, D. A., J. M. Cabral, R. A. Pfuetzner, A. Kuo, J. M. Gulbis, S. L. Cohen, B. T. Chait, and R. MacKinnon.** The structure of the potassium channel: molecular basis of K^+ conduction and selectivity. *Science* 280: 69–77, 1998.
5. **Drewe, J. A., S. Verma, G. Frech, and R. H. Joho.** Distinct spatial and temporal expression patterns of K^+ channel mRNAs from different subfamilies. *J. Neurosci*. 12: 538–548, 1992.
6. **Dveksler, G. S., A. A. Basile, and C. W. Dieffenbach.** Analysis of gene expression: use of oligonucleotide primers for glyceraldehyde-3-phosphate dehydrogenase. *PCR Methods Appl*. 1: 283–285, 1992.
7. **Francke, U.** Digitized and differentially shaded human chromosome ideograms for genomic applications. *Cytogenet. Cell Genet*. 65: 206–218, 1994.
8. **Guan, X. Y., J. Xu, S. L. Anzick, H. Zhang, J. M. Trent, and P. S. Meltzer.** Hybrid selection of transcribed sequences from microdissected DNA: isolation of genes within amplified region at 20q11-q13.2 in breast cancer. *Cancer Res*. 56: 3446–3450, 1996.
9. **Hugnot, J. P., M. Salinas, F. Lesage, E. Guillemare, J. de Weille, C. Heurteaux, M. G. Mattei, and M. Lazdunski.** Kv8.1, a new neuronal potassium channel subunit with specific inhibitory properties towards Shab and Shaw channels. *EMBO J*. 15: 3322–3331, 1996.
10. **Isacoff, E., D. Papazian, L. Timpe, Y. N. Jan, and L. Y. Jan.** Molecular studies of voltage-gated potassium channels. *Cold Spring Harb. Symp. Quant. Biol*. 55: 9–17, 1990.
11. **Kozak, M.** An analysis of 5′-noncoding sequences from 699 vertebrate messenger RNAs. *Nucleic Acids Res*. 15: 8125–8148, 1987.
12. **Kramer, J. W., M. A. Post, A. M. Brown, and G. E. Kirsch.** Modulation of potassium channel gating by coexpression of Kv2.1 with regulatory Kv5.1 or Kv6.1 α-subunits. *Am. J. Physiol*. 274 (*Cell Physiol*. 43): C1501–C1510, 1998.
13. **Kyte, J., and R. F. Doolittle.** A simple method for displaying the hydropathic character of a protein. *J. Mol. Biol*. 157: 105–132, 1982.
14. **Lurie, I. W., H. G. Ilyina, D. B. Gurevich, N. V. Rumyantseva, I. V. Naumchik, C. Castellan, A. Hoeller, and A. Schinzel.** Trisomy 2p: analysis of unusual phenotypic findings. *Am. J. Med. Genet*. 55: 229–236, 1995.
15. **MacKinnon, R., and G. Yellen.** Mutations affecting TEA blockade and ion permeation in voltage-activated K^+ channels. *Science* 250: 276–279, 1990.
16. **Milner, R. D., K. A. Khallouf, R. Gibson, A. Hajianpour, and C. G. Mathew.** A new autosomal recessive anomaly mimicking Fanconi's anaemia phenotype. *Arch. Dis. Child*. 68: 101–103, 1993.
17. **Nakahira, K., G. Shi, K. J. Rhodes, and J. S. Trimmer.** Selective interaction of voltage-gated K^+ channel beta-subunits with alpha-subunits. *J. Biol. Chem*. 271: 7084–7089, 1996.
18. **Patel, A. J., M. Lazdunski, and E. Honore.** Kv2.1/Kv9.3, a novel ATP-dependent delayed-rectifier K^+ channel in oxygen-sensitive pulmonary artery myocytes. *EMBO J*. 16: 6615–6625, 1997.
19. **Post, M. A., G. E. Kirsch, and A. M. Brown.** Kv2.1 and electrically silent Kv6.1 potassium channel subunits combine and express a novel current. *FEBS Lett*. 399: 177–182, 1996.
20. **Rae, J. L., and R. A. Levis.** Glass technology for patch clamp electrodes. *Methods Enzymol* 207: 66–92, 1992.
21. **Rae, J. L., and A. R. Shepard.** Identification of potassium channels in human lens epithelium. In: *Current Topics in Membranes*. San Diego, CA: Academic, 1998, p. 69–104.
22. **Rae, J. L., and A. R. Shepard.** Molecular biology and electrophysiology of calcium-activated potassium channels from lens epithelium. *Curr. Eye Res*. 17: 264–275, 1998.
23. **Rothschild, C. B., G. Akots, R. Hayworth, M. J. Pettenati, P. N. Rao, P. Wood, F. M. Stolz, I. Hansmann, K. Serino, and T. P. Keith.** A genetic map of chromosome 20q12-q13. 1: multiple highly polymorphic microsatellite and RFLP markers linked to the maturity-onset diabetes of the young (MODY) locus. *Am. J. Hum. Genet*. 52: 110–123, 1993.
24. **Saal, H. M., L. J. King, D. Zimmerman, R. C. Johnson, A. G. Carr, C. A. Samango-Sprouse, and W. Stanley.** Loss of the N-myc oncogene in a patient with a small interstitial deletion of the short arm of chromosome 2. *Am. J. Med. Genet*. 66: 373–377, 1996.
25. **Salinas, M., J. de Weille, E. Guillemare, M. Lazdunski, and J. P. Hugnot.** Modes of regulation of shab K^+ channel activity by the Kv8.1 subunit. *J. Biol. Chem*. 272: 8774–8780, 1997.
26. **Salinas, M., F. Duprat, C. Heurteaux, J. P. Hugnot, and M. Lazdunski.** New modulatory alpha subunits for mammalian Shab K^+ channels. *J. Biol. Chem*. 272: 24371–24379, 1997.
27. **Sambrook, J., E. F. Fritsch, and T. Maniatis.** *Molecular Cloning: A Laboratory Manual* (2nd ed.). Cold Spring Harbor, NY: Cold Spring Harbor, 1989.
28. **Shepard, A. R., and J. L. Rae.** Ion transporters and receptors in cDNA libraries from lens and cornea epithelia. *Curr. Eye Res*. 17: 708–719, 1998.
29. **Shepard, A. R., and J. L. Rae.** Magnetic bead capture of cDNAs from double-stranded plasmid cDNA libraries. *Nucleic Acids Res*. 25: 3183–2185, 1997.
30. **Splawski, I., K. W. Timothy, G. M. Vincent, D. L. Atkinson, and M. T. Keating.** Molecular basis of the long-Qt syndrome associated with deafness. *N. Engl. J. Med*. 336: 1562–1567, 1997.
31. **Stocker, M., and D. Kerschensteiner.** Cloning and tissue distribution of two new potassium channel alpha-subunits from rat brain. *Biochem. Biophys. Res. Commun*. 248: 927–934, 1998.
32. **Wible, B. A., Q. Yang, Y. A. Kuryshev, E. A. Accili, and A. M. Brown.** Cloning and expression of a novel K^+ channel regulatory protein, KChAP. *J. Biol. Chem*. 273: 11745–11751, 1998.
33. **Winsor, S. H., M. J. McGrath, M. Khalifa, and A. M. Duncan.** A report of recurrent anencephaly with trisomy 2p23–2pter: additional evidence for the involvement of 2p24 in neural tube development and evaluation of the role for cytogenetic analysis. *Prenat. Diagn*. 17: 665–669, 1997.